



AirCargoChallenge 2022

Technical Report

Team #12

AeroUD

AeroUD

Mechanical

Engineering

Team



Contents

List of Symbols	II
1 Introduction	1
2 Project Management	2
2.1 Team organization and activity scheduling	2
2.2 Budget management	3
3 Aerodynamic Design	4
3.1 Propeller Test	4
3.2 Wing design criteria	5
3.3 Empennage design static margin definition	10
3.4 Fuselage and cargo-bay	11
4 Structural Design	12
4.1 Wing structure	13
4.2 Fuselage, landing gears and engine pod	14
4.3 Tail boom and empennages	16
4.4 Construction process	17
5 Electronics	18
5.1 Battery sizing	18
5.2 Servomotor sizing	19
5.3 Flight Telemetry	21
6 Optimization process	23
6.1 The first prototype BcdM1	23
6.2 The second prototype PH1	23
7 Payload prediction	25
8 Outlook	26

List of Symbols

A_r	wing aspect ratio [-]
A_w	wing surface [m ²]
b	wingspan [mm]
C	battery capacity [mAh]
C_{aero}	Pitching moment acting on the tail [Nm]
$C_{d,0}$	fuselage, tail and landing gear drag coefficient [-]
$C_{d,2D}$	drag coefficient from 2D calculations [-]
$C_{d,tot}$	airplane total drag coefficient [-]
$C_{l,mac}$	Lift coefficient at the aerodynamic medium chord [-]
$C_{l,2D}$	lift coefficient from 2D calculations [-]
$C_{l,tot}$	airplane total lift coefficient [-]
C_{servo}	Torque required to the servo [Nm]
D	drag force [N]
I	current [A]
L	lift force [N]
L_c	control surface average length [m]
mac	medium aerodynamic chord [mm]
$MTOW$	maximum take-off weight [gr]
P	predicted payload [kg]
SM	static margin [-]
v	aircraft speed [m/s]
X_{cg}	distance of the center of gravity from the leading edge [mm]
X_{np}	distance of the neutral point from the leading edge [mm]
y	semi-wingspan distance from the wing root [m]
α	angle of attack [rad]
β	maximum servo deflection [rad]
γ	maximum control surface deflection [rad]
ρ	air density [kg/m ³]



1 Introduction

At the University of Udine, the participation at the Air Cargo Challenge (ACC) competition is a well-established and renowned opportunity for the students of the engineering courses to experience firsthand a working oriented environment, where all the notions obtained during lessons have to be put in practice. Despite the handicap of not having a dedicated aeronautical engineering course, and indeed all the teams' members were and are either mechanical or electronic engineering students, the AeroUD teams have always been able to rank in high positions. In particular, in the 2019 edition both teams were able to hit the podium missing the final victory by just a handful of points.

In April 2020 a new team was founded, and thanks to the economic support given by our university, it was decided to take part in the actual edition of the competition. Because of the pandemic outburst of Coronavirus, the competition had to be postponed to 2022 and some members who graduated had to be replaced. The pandemic posed also a large number of organizational problems, which inevitably slowed down the project. For many months of the 2020 it was impossible to meet in person and work efficiently on the design of the model. Successively, the access to the University Labs was limited to two team members at the time, and the construction phase suffered of the lack of manpower. Despite all these difficulties, the new AeroUD model PH-2 has been design, built and successively optimized and is ready to fly in Munich next July.

The design activities started with some preliminary tests that were made on the propellers indicated by the regulations. The analysis aimed to find the best propeller in terms of traction for the flight envelope, and this value was one of the most important input data for the aerodynamic design. At the end of this design phase (carried out with a simple procedure but that proved to be effective), a first prototype (BcdM1) was built in order to validate the overall concept. In this first attempt, attention was mainly paid in the realization of the aerodynamic surfaces of the main wing and of the tail, while the fuselage (i.e. the cargo bay) was just a big and cheap wooden box. This approach was chosen to keep as low as possible both building time and costs. Flight tests of the prototype carried out in autumn 2020 revealed performance in agreement with the design target and therefore wing and tail geometry were frozen and the attention was dedicated to the fuselage, engine and battery pod, landing gears, etc. The most important requirements for their design were obviously the lighter as possible weight and aerodynamically efficient shapes. In October 2021 a second prototype, PH-1, was maiden and an intensive flight campaign, simulating the race flight mission, was accomplished within the successive three months. The large amount of data collected helped the team to further optimize the design for some important aspects (e.g. cargo bay dimension, adoption of wing flaps) and to figure out a first race strategy. At the time when this document is written (March 2022), the final model is under construction and the maiden flight is foreseen in few weeks. Flight tests will follow until the race day, this in order to fine tune the airplane settings and consolidate a race strategy.

This report aims at documenting as thoroughly as possible the long journey above described.

2 Project Management

This section is devoted to a brief description of team management in terms of time schedule and activity planning and it will also provide an overview of the budget.

2.1 Team organization and activity scheduling

The recruitment of the team started in the end of 2019 and probably on the wave of the success the AeroUD team had in the previous ACC competition, at the beginning a large number of students joined the challenge. The team was indeed originally composed by 12 students and therefore it was decided to organize the team into three working groups with the following tasks:

- aerodynamic division: design the main aerodynamic surfaces of the aircraft;
- structural design and drawings division: model the external surfaces of the plane (except the main wing and the tail) and the internal structure of the aircraft's components;
- electronics and propulsion system division: in charge to select all the electronic components and to develop a real time telemetry.

The team leader was also responsible for budget management while the construction and flight tests were carried out by all team members.

Because of COVID-19 regulations the team initially worked mostly online or in small groups in the laboratory. This, together with the announcement of the competition postponement of 1 year, smoothed down the enthusiasm of some of the participants. Some of them will also have been graduated before 2022. The number of team members drastically reduced to 6 and the team had to reformulate its targets and ambitions.

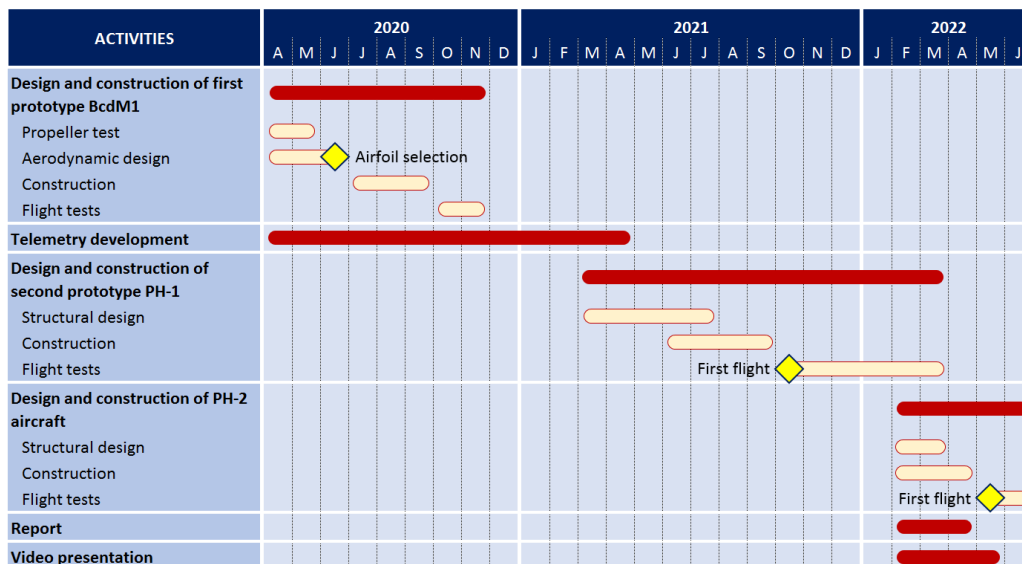


Figure 1: Gantt diagram of the project

The main activities of the projects can be summarized as it follows. The first 12 months were devoted to the aerodynamic design of a final configuration of wing and tail and to the construction of a first prototype used to proof the validity of the design. Successively, the attention was focused on the design of a second prototype, optimizing also to structure weight and overall aerodynamics.

This second prototype was used to test performance in race mode, analyze the data and make the final optimization to improve performances. At present time the race model (PH2) is under construction and its maiden flight is foreseen for the end of April. The remaining time until the race will be used to realize the video presentation and to define a race strategy. A detailed view of the project schedule can be obtained by the Gantt chart in Fig. 1.

2.2 Budget management

At the beginning of the project, the team made a first estimation of the required budget. This was done knowing the budgets spent in the previous edition but also considering that:

1. need to design and build at least two prototypes and a race model;
2. the prototypes could use most of the electronic components from the previous edition;
3. mould manufacturing was not a cost anymore (exception done for the raw material), the laboratory has a new CNC machine suited for the purpose;
4. travel costs are reduced to a minimum since Munich can be easily reached by car from Udine.

Table 1: Budget overview

First prototype BcdM1	Construction material wing moulds	€ 200
	Construction material - general (glass fibre tissue, epoxy resin, PVC foam, 3D printed components, etc)	€ 400
	Electronics (batteries, ESC and GPS unit)	€ 400
	Subtotal	€ 1'000
Second prototype PH1	Construction material fuselage and tail moulds	€ 200
	Construction material - general (glass and carbon fibre tissue, epoxy resin, PVC foam, 3D printed components, carbon tubes, etc)	€ 1'500
	Subtotal	€ 1'700
Race model PH2	Construction material - general (glass and carbon fibre tissue, epoxy resin, PVC foam, 3D printed components, carbon tubes, etc)	€ 1'500
	Electronics (new servos, batteries, engine)	€ 500
	Subtotal	€ 2'000
Travel Cost	Competition Fee	€ 1'800
	Transfer by car to/from competition	€ 1'500
	Subtotal	€ 3'300
Others	Team uniforms	€ 1'000
	External services for marketing material	€ 1'000
	Subtotal	€ 2'000
Total		€ 10'000
10% of contingencies		€ 1'000
TOTAL OF THE PROJECT		€ 11'000

The financial support provided by the University for the 2020-2022 AeroUD project was 8'000 euros. The team therefore realized immediately the necessity to find sponsors to reach financial sustainability. This target was achieved at the end of 2021 when two local companies decided to give support to the team by sponsoring the team Uniforms and the purchases of some material for a value of roughly 2'000 euros. At present, the foreseen budget has however been respected. Savings have been made in the majority of the voices and the 10% safety margin is still untouched.

3 Aerodynamic Design

Before to describe in detail the design procedure, some preliminary considerations are required. The constraints and score rules imposed by the regulations that have a stronger impact on the aerodynamic design are:

- the aircraft must fit into a rhombus with a side of 1500 mm, limiting consequently the maximum dimension of the plane;
- payload capacity and climbing rate are requested at the same time;
- the low density of the payload might require very large cargo bay which might penalize the overall aerodynamic performances;
- limited traction available at the propeller;
- take-off from a grass runway.

A bi-plane configuration was initially considered as an option to guarantee high payload within the imposed small dimensions of the airplane, but at the end it was disregarded. Indeed, the bi-plane configuration has the advantage to carry more payload but, from the flight mission simulation this advantage in payload turned into strong limitations in speed and reached altitude. Therefore, a classical monoplane high wing configuration was selected, configuration that based on the team experience from the past ACC is also the most reliable and stable when high payloads (relatively to the empty weight) are requested. To ease the take-off from grass runway, a tail dragger landing gear configuration was preferred to the three-cycle one, even if it might pose some issues related to handling strong cross wind during take-off.

3.1 Propeller Test

The first step towards the aerodynamic design was testing and figuring out the best propeller available for this year's competition between the APC-E 10x6E and the Aeronaut CAMcarbon Light 10x6. The choice was made by using as a figure of merit the traction provided by the propellers in various working conditions. To accomplish this task, a test bench developed for the previous ACC competitions was used, see Fig. 2.

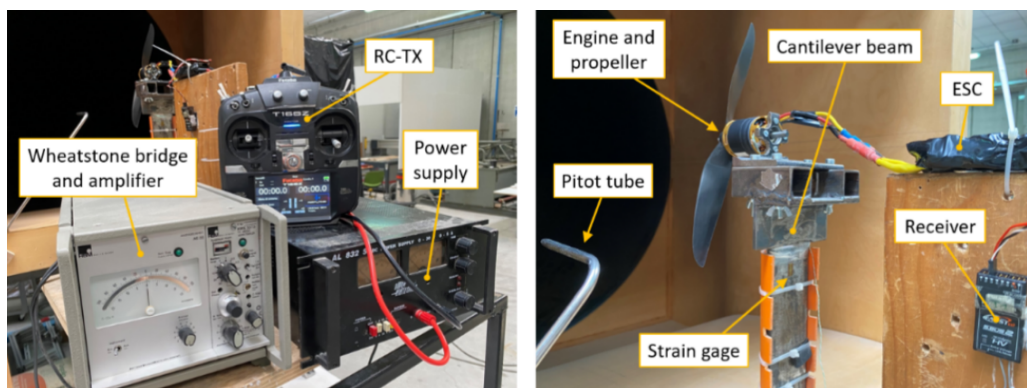


Figure 2: Test bench used to select the best propeller for the competition

In the test bench, the propeller traction is measured by mounting the engine on the free end of cantilever beam. The small bending of the beam due to the action of propeller is measured by means of strain gauges fixed on the clamped side of the beam. The data were acquired simulating different flight speeds in between 0 and 25 m/s by placing the system in front the exit of and open loop wind tunnel and by powering the engine controller at the fixed voltage of 11.5 V, 12 V, and 12.5 V. The results are shown in Fig. 3.

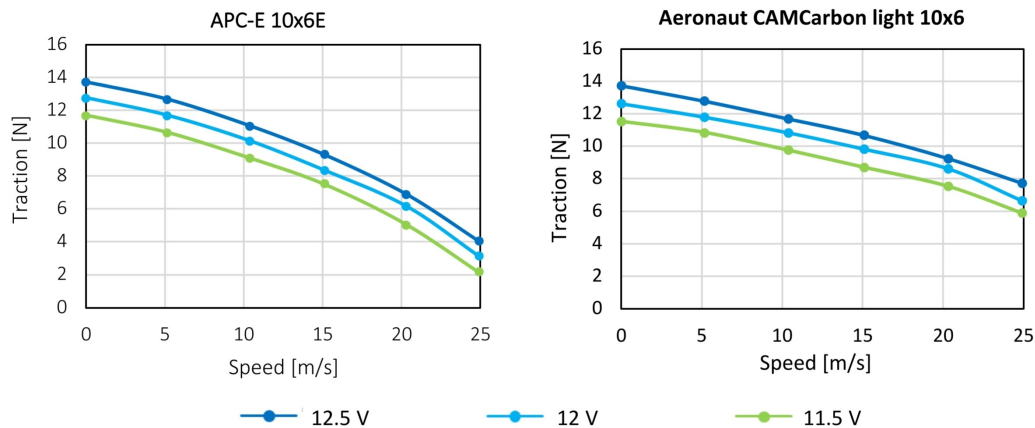


Figure 3: Propeller's traction at variable air flow speed and supply voltage to the motor ESC

The graphs show that the Aeronaut CAMcarbon Light 10x6 has a higher traction compared to the APC-E 10x6E in all the working conditions, and therefore it was chosen for the project. The experimental data were successively interpolated in the 3D space traction/air speed/voltage and used as input for the following aerodynamic design. While taking the traction measurements, the current absorption of the motor was also acquired; this data have been used to determine the battery capacity and discharge rate (see Section 5.1).

3.2 Wing design criteria

This paragraph is dedicated to the description of the methodology that is at the core of the wing aerodynamic design. Being the team composed by student with no specific background in aerospace engineering, a very simple approach has been pursued. However, satisfactory performances were reached in a first prototype design, leaving further optimizations based on the experimental evidence from flight tests.

The methodology is articulated in successive steps that are repeated for multiple airfoil geometries as described in the following and graphically shown in Fig. 4:

1. identification of a candidate airfoil for the wing;
2. numerical determination of the airfoil 2D polars at variable Reynolds numbers and angles of attack;
3. determine the performances (Lift and Drag) of a rectangular planform wing of variable chord and wingspan within the imposed dimension limitations and at variable angle of attack;
4. select the best wing planform based on the value of an ad-hoc defined score function;
5. repeat steps 1-4 for different airfoils;
6. select the best performing wing;
7. final 3D wing numerical simulation with wing loading optimization.

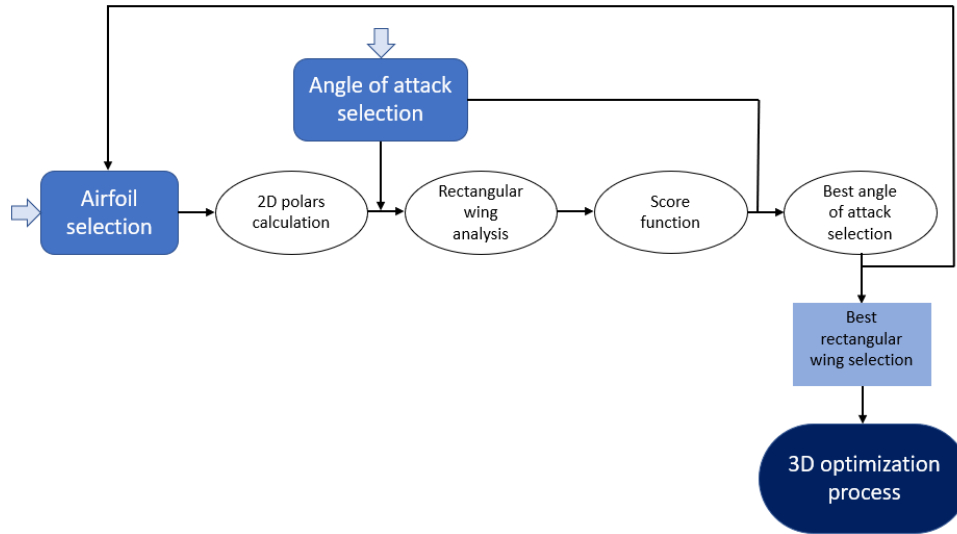


Figure 4: Flow chart of the wing aerodynamic design procedure

For a given airfoil geometry, the 2D polars at variable Reynolds number (in the range 100'000-700'000) are computed by means of the free software XFLR5.

The polars data are then used to compute Lift and Drag coefficients of a rectangular planform wing by applying the formulas:

$$C_{d,tot} = C_{d,0} + C_{d,2D} + \frac{C_{l,tot}^2}{\pi \cdot A_r \cdot 0.8} \quad (1)$$

$$C_{l,tot} = \frac{C_{l,2D}}{1 + \frac{C_{l,2D}}{\pi \cdot A_r \cdot 0.8}} \quad (2)$$

The term $C_{d,0}$ in Eq. (1) is used to account for the drag caused by the airframe components except the wings (fuselage, landing gears, etc.) and its correct estimation is crucial for a good design. Unfortunately, it is not an easy task to define the $C_{d,0}$ value without relying on complex 3D viscous simulations or wind tunnel experimental tests. Both options were obviously not affordable by the team in view of the costs, time and skills required. The only reasonable option was to profit of the team knowledge gained in the previous ACC and assume as a first tentative value the $C_{d,0}$ of one of the models that competed in the 2019 edition. That value (0.043) was fine-tuned on the basis of experimental tests on a dedicated prototype.

The next step of the procedure requires to compute the Lift and Drag of the wing by means of:

$$D = \frac{1}{2} \cdot \rho \cdot C_{d,tot} \cdot A_w \cdot v^2 \quad (3)$$

$$L = \frac{1}{2} \cdot \rho \cdot C_{l,tot} \cdot A_w \cdot v^2 \quad (4)$$

where the flight speed is required. This latter can be obtained assuming a condition of levelled horizontal flight where drag and propeller traction are equal. The propeller traction obtained as described in Section 3.1 is also a function of the flight speed. Therefore, an iterative procedure is needed to compute the forces acting on the wing and the flight speed.

After doing this, the wing under consideration must be ranked in terms of race performance. The ACC2022 scoring rules are defined on three parameters: lifted payload, altitude reached in 60 seconds after take-off, and travelled distance in 120 seconds. The first and the second one mainly depends on the lift, while the travelled distance is proportional to the aircraft's speed. Therefore, an optimum problem is posed because a wing that is designed to maximize the payload lifted leads necessarily to a high drag coefficient and so the speed cannot be very high. Therefore, a score function that weights equally both speed and lift seem to be the best choice:

$$SCORE = L \cdot v \quad (5)$$

The score is computed for a family of rectangular wing planform so obtaining a score matrix as the one reported as an example in Fig. 5.

S= L*v		wingspan [m]								
		1,5	1,6	1,7	1,8	1,9	2	2,1	2,2	2,3
chord [m]	0,1	0,352	0,373	0,394	0,415	0,435	0,455	0,475	0,495	0,514
	0,12	0,431	0,458	0,484	0,509	0,535	0,560	0,584	0,610	0,633
	0,14	0,498	0,528	0,559	0,589	0,618	0,647	0,677	0,707	0,733
	0,16	0,551	0,586	0,619	0,653	0,686	0,718	0,751	0,786	0,814
	0,18	0,594	0,631	0,668	0,704	0,739	0,775	0,811	0,849	0,878
	0,2	0,627	0,666	0,705	0,743	0,781	0,818	0,856	0,898	0,927
	0,25	0,678	0,720	0,761	0,802	0,843	0,883	0,926	0,971	1,000

Figure 5: Example of score matrix for a given profile and incidence angle normalized with respect the best score

The same calculation is repeated by varying the wing angle of attack, and from the series of performance matrices, the best performing wing is selected.

The procedure above described was repeated for different airfoils selected from the available data base. The guidelines used for airfoil selection were:

- airfoil design for low Reynolds number operation;
- availability of polar data at least for two values of Reynolds number falling inside the design range (100'000-700'000), this in order to validate the numerical predictions;
- high lift and low drag;
- low moment coefficient, which limit the request of large tail surfaces or long tail booms, which is seen as an advantage to reduce the overall drag and airplane weight.

By comparing the results obtained in the matrices for a family of airfoils, it was clear how the score always increases for larger chords and wingspan and using higher angles of attack. Nevertheless, it was decided not to choose the configuration with maximum score because of the low density of the

blood bags used as a payload. Indeed, it turned out the score increases mainly by the contribution of the payload value (the lift of the wing): higher payload means bigger cargo bay with a consequent unavoidable draw back in the aerodynamic efficiency of the fuselage (increase in the value of $C_{d,0}$ above mentioned). This would have been translated into a maximum speed penalization. It was therefore decided to choose a maximum take-off weight of about 6000 g that is a good trade-off to optimize both payload and travelled distance. The limit was chosen assuming a first layout of the blood bags inside the cargo bay and the maximum dimensions of this latter (more details about cargo bay in Section 4.2).

Made these considerations and after a thorough data evaluation, the best configuration was obtained using a wing of 350 mm of chord and 2100 mm of wingspan, shaped with the WFX 63-137 airfoil shown in Fig. 6.

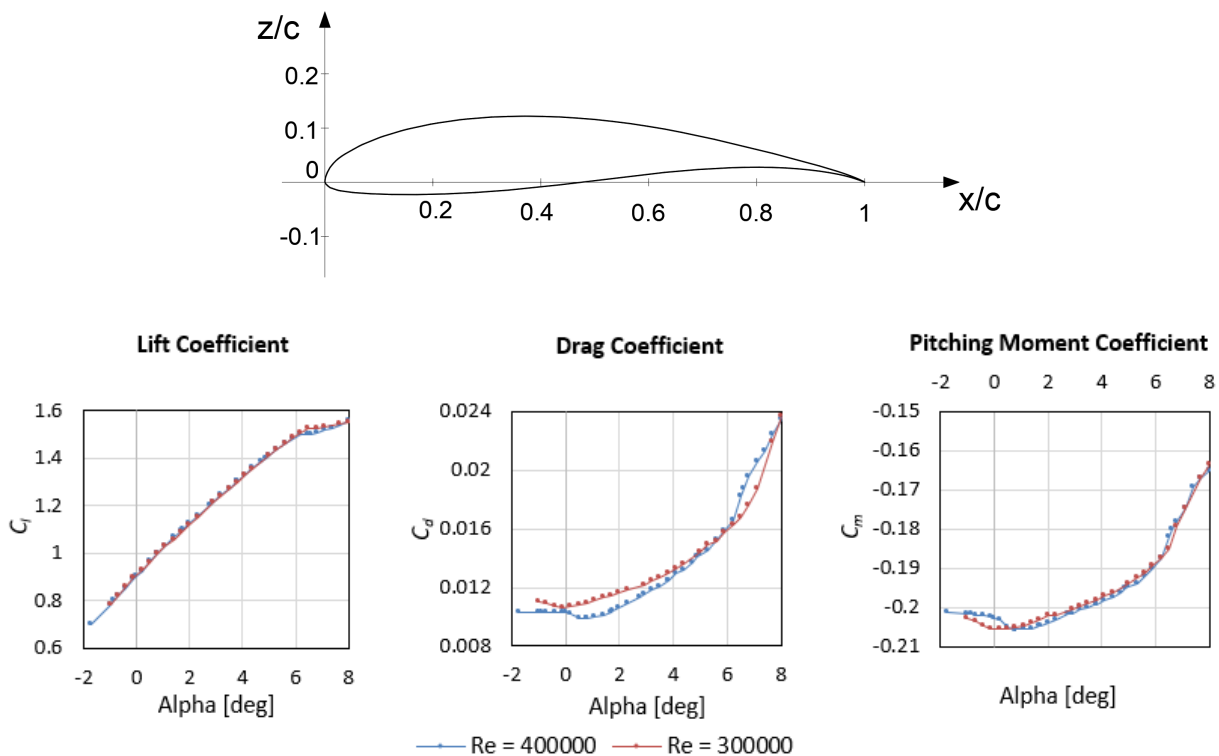


Figure 6: The selected airfoil WFX 63-137 and its 2D polar data for two values of the Reynolds number

The final step of the wing aerodynamic design procedure requests to optimize the wing planform in order to limit the induced drag effects localized at the wing tips and to obtain an elliptical load distribution, according to the Schrenk criterion.

The wing loading is defined as:

$$loading(y) = Chord(y) \cdot \frac{C_l(y)}{mac} \quad (6)$$

According to the Schrenk criterion, the wing loading can be described in Eq. (7).

$$Elliptic\ loading(y) = \frac{C_l(y)}{mac} \frac{4A_w}{\pi b} \sqrt{1 - \left(\frac{2y}{b}\right)^2} \simeq \frac{C_{l,max}}{mac} \frac{4A_w}{\pi b} \sqrt{1 - \left(\frac{2y}{b}\right)^2} \quad (7)$$

where:

- mac represents the aerodynamic medium chord;
- y represents the semi-wingspan distance from the wing root;
- $C_l(y)$ is the lift coefficient in function of y ;
- b is the wingspan;
- A_w is the wing area.

To obtain a load distribution as much as possible according to the Schrenk criterion an elliptical taper for the wing planform was adopted. The leading edge moves backwards according to the equation of an ellipse, while the trailing edge is kept as a straight line, to facilitate the installation of both ailerons and flaps.

Induced drag and stall behavior were both mitigated also by staggering nose down the wing tips.

Multiple attempts were made and the wing loading distribution computed with XFLR5 compared with the theoretical one until a satisfactory geometry was identify. The resulting geometry is sketched in Fig. 7 while the resulting wing loading is shown in Fig. 8. The airfoil angle of attack is 2 deg at wing root and varies linearly down to 0 deg mowing towards the tip.

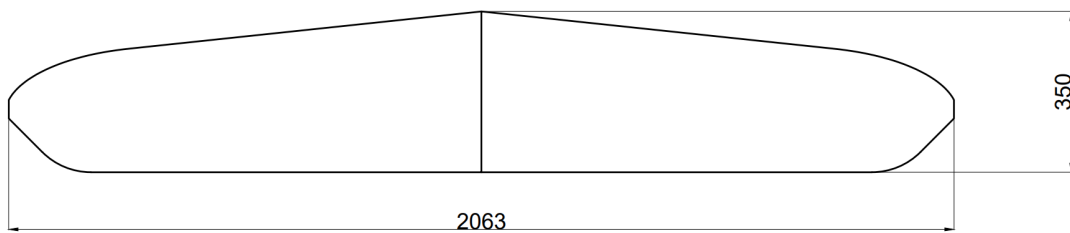


Figure 7: The selected wing planform

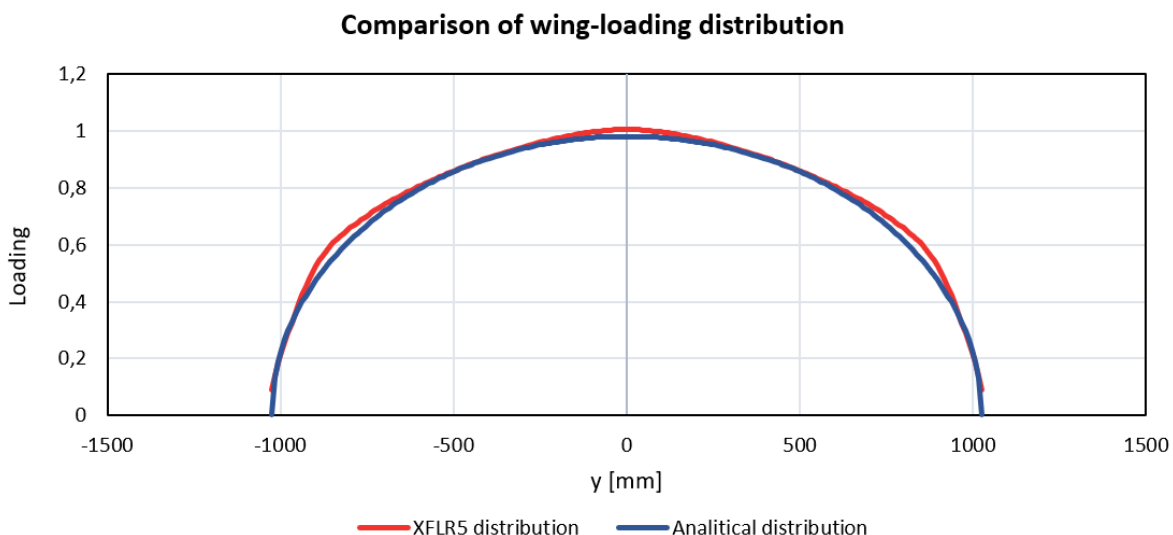


Figure 8: Wing loading distribution

3.3 Empennage design static margin definition

To correctly size the tail of the plane, the capabilities of the XFLR5 program were again exploited, since it can also provide static stability calculations. The team decided to adopt a V-tail full fling configuration because it has an excellent manoeuvrability and efficiency, not only in the controls but also in possible stability control trimmers, during the use of the flaps; a reduction of the overall drag of the tail is possible with respect a more conventional “T” and flapped configuration.

The adopted airfoil for the empennage is the symmetrical NACA 0009, which is characterized by a very low drag coefficient, maintaining a significant thickness per quarter of chord. This feature has been fundamental in terms of construction, in order to have enough space for both servos and spars installation. The tail stagger angle was set at zero degrees, to limit its contribution to drag as much as possible.

The geometry chosen for the empennages was found starting from the dimensions of the main wing through correlations from literature (Daniel P. Raymer, Aircraft Design: A Conceptual Approach, 4th edition). This analysis provided a total surface of 0.149 m^2 , area that can be obtained with a trapezoidal planform with chord of 202.5 mm and of 130.5 mm at the root and tip, respectively, and a length of 450 mm. The dihedral angle was chosen at 45 deg. However, limitations due to the box where the model must fit while standing on its landing gear (dimensions 1.5·1.5·0.5 m) did not allow to adopt this shape. The tail was therefore reshaped as shown in Fig. 9 and a 10% reduction of the surface to 0.1374 m^2 was also necessary.

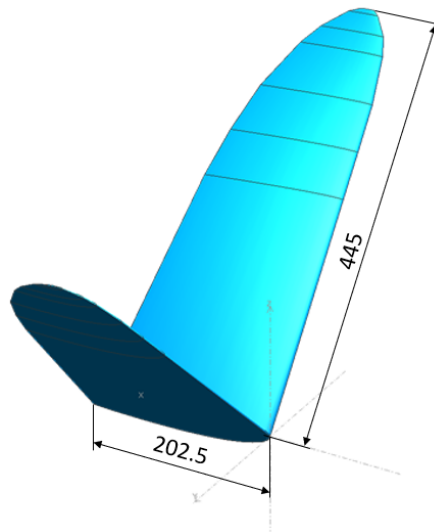


Figure 9: Empennage planform

The position of the tail (i.e. the length of the tail boom) was chosen at the maximum distance from the wing leading edge within the limit of the of the box above mentioned. The final aerodynamic surface configuration is shown in Fig. 10.

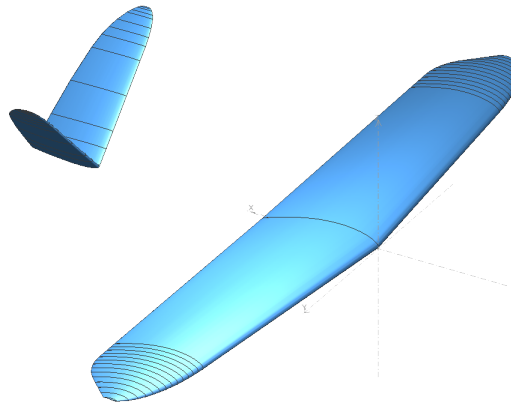


Figure 10: 3D view of the aerodynamic surfaces layout

Once the tail geometry was fixed, it was necessary to check for the static stability, which is ensured as long as the static margin is positive. The static margin is a dimensionless coefficient defined as:

$$SM = \frac{X_{np} - X_{cg}}{mac} \quad (8)$$

where X_{np} is the neutral point and X_{cg} is the centre of gravity (CG), both calculated with reference to wing leading edge at the root. This latter was unknown at this stage of the design and therefore it was decided to impose a target SM and to compute the X_{cg} value that ensure the desired static stability. The static margin was set at 13%, judged as a good compromise between stability and manoeuvrability. The results of the stability analysis are summarized in Tab. 2.

Table 2: Results of the static stability calculation performed with XFLR5

X_{np} [mm]	X_{cg} [mm]	mac [mm]	SM [-]
91.427	157	264.823	13%

The value of X_{cg} in the Tab. 2 has been therefore fixed and the design of the airplane had to respect it. In particular no variation of CG is admissible at variable payload. This target was achieved with an ad-hoc design of the cargo bay as commented in the next section.

3.4 Fuselage and cargo-bay

The fuselage has to be large enough to host the blood bags. The general criteria for the design of the fuselage was to keep as low as possible its aerodynamic drag and the negative interaction with the wings. In particular, to minimize this effect, it was decided to connect the fuselage to the wings by means of a fin (see Fig. 14). The latter is externally shaped as a NACA 0020 profile, which is thick enough to allow the installation of the internal structure that is necessary to withstand the mechanical loads, mostly associated to the payload inertia. At the same time, particular care was put in the design of the external surfaces in order to keep them as aerodynamically efficient as possible. The calculated position of the CG (fixed for every payload configuration and obtained from static stability analysis) was used as an additional input for the fuselage design. Indeed, the intention was to design a fuselage with a cargo bay with its geometrical centre coincident with the CG position and

capable to host the blood bags always in a symmetric configuration with respect the CG. By doing so, airplane CG and its stability is not affected by the payload amount at take-off. The final cargo bay configuration is capable to host 12 bags of 300 g organized inside 3 different compartments to avoid dangerous payload movements during flight. More details of the fuselage and cargo bay internal structures are provided in Section 4.

4 Structural Design

This section is dedicated to description of the airframe internal structure, how it was chosen and built.

The team opted to rely on composite materials for the construction of the whole aircraft. This because:

- composite materials ensure some of the lowest weight-per-rigidity ratio, a mandatory characteristic in search of maximum performance;
- lamination of composite materials results in excellent surface finishing;
- through proper mould machining, complex shapes can be manufactured, allowing smooth and aerodynamically sensible couplings of the various components.

These considerations put together would end up in the best result in search of performance.

Accurate structural design of composite materials can be a hard task to be achieved also by the most advanced numerical tools that are available to engineers. This in view of the anisotropic behaviour of these artifacts, especially when sandwiches of different types of materials are used. However, in this specific project, the mechanical loads to be carried by the structures are very low because:

- airplane wingspan is limited by regulations to a maximum of 2100 mm;
- small dimension of the model and low propeller traction available imply low maximum take-off weight (MTOW, in this case estimated to 6000 g);
- no need to make sharp turns or manoeuvres during flight that could bring to high accelerations, the highest load conditions for the wing would be the static test to be performed before each flight attempt.

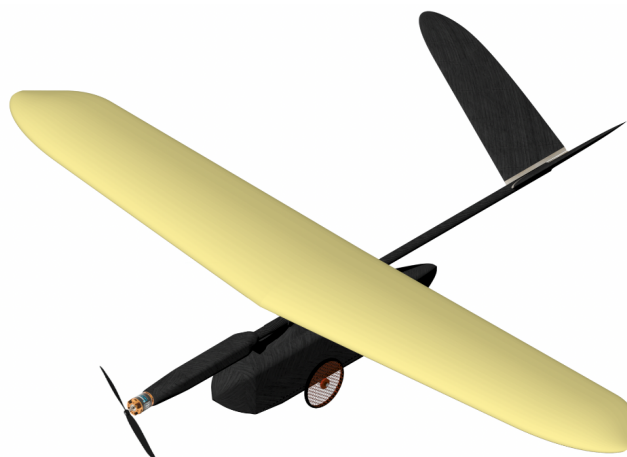


Figure 11: Final airframe

After the considerations of above and base on the team experience (in the previous project a model of about 5 m wingspan and with a MTOW of 17 kg was successfully realized), it was immediately clear that the mechanical loads (less than 30 Nm of maximum bending moment at the wings) would not represent an issue and that they could be withstand by a very light composite structure without the need of a preliminary sizing. The attention in the structural design was therefore turned to the definition of an airframe as light and as aerodynamically efficient as possible, leaving the verification of the mechanical resistance by experimental tests on the manufactured model.

The resulted airframe is depicted in Fig. 11.

4.1 Wing structure

The expected loads from the dynamics of flight include two main moments applied to the wing, a bending moment and a torque. The torque is supported exclusively by the skin of the wing, while the bending moment, the most critical, is supported by both wing skin and wing spar.

The wing skin (see Fig. 12) consists of a sandwich made by bidirectional glass fibre fabric of 25 g/m² weight, 2 mm thickness PVC foam (Airex@M060), glass fibre fabric of 25 g/m² weight. The glass fabric has the fibre oriented ± 45 deg with respect to the wingspan direction, i.e. in the direction aligned with the torque moment. The wing spar connects the two skins (suction and pressure side of the airfoil) and is again made by a sandwich of 2 layer of the same PVC foam alternated with 3 layers of bidirectional glass fibre fabric 25 g/m² weight. In this case the glass fibres are obviously aligned along the wingspan direction (and 90 deg to it). High quality epoxy resin is used as bonding and matrix for the fabrics, the sandwiches are obtained with the vacuum moulding technique (see later for more details).

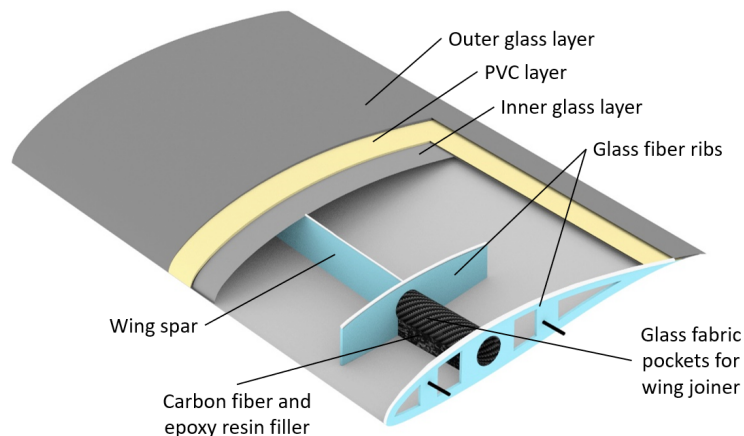


Figure 12: Wing internal structure

It is worth to mention that the aileron hinges are realized directly on the suction side skin during the moulding process and by means of a peel ply fabric (50 g/m²) layered in between the external glass fabric and the PVC foam.

The wing is realized in two sections of about 978 mm, and they join together by means of a carbon fibre tube that insert inside glass fabric pockets. These latter are kept in place inside the wing structure by two ribs, one at the root and one 90 mm inside. To transfer the bending moment from the wing structure to the carbon tube, the space in between the tube pockets and the wing skin

is filled with epoxy resin mixed with hollow glass microspheres (2.5 g/cm^3). The carbon tube is a commercial one of 26 mm diameter and 0.7 mm thickness.

Once the structure has been realized, a bending test has been executed by simulating the static load test the wing will have to resist at the competition. The two semi-wings, joined by the tube, were suspended at both tips and a lead load of 7500 g was connected at the centre (i.e. a load higher than the expected MTOW of 6000 g), see Fig. 13.



Figure 13: Wing undergoing load static test with 7500 g

Wing bending displacement was limited to 20 mm and no evidence of bending instability of the skin or failure was detected. This structure that weight only 600 g including the connection tube, proved to be reliable also by many flights performed by the PH1 prototype at MTOW. Most likely, there is still margin for improvement in the weight, but the already mentioned organizational difficulties that the team had to face did not allow dedicating more time to this aspect of the design.

4.2 Fuselage, landing gears and engine pod

The fuselage must fulfill many requirements:

- allow an easy and fast payload loading;
- it must be able to withstand the acceleration forces on the payload during the flight;
- in the present configuration, it must be able to house the landing gear and therefore withstand the landing loads;
- minimal cross section and aerodynamic shape in order to limit drag.

The cargo bay is accommodated inside a pod suspended to the wing by a pedestal. This latter is the most critical component since it has to transfer the inertial forces acting on the payload during flight to the wing and it is also subjected to impulsive loads at landing. The internal structure of the pedestal is sketched in Fig. 14 that reports a sectional view of the structure under discussion.

A structure made of ribs and frames in composite sandwich, covered with a layer of carbon fabric resulted the best choice. The pedestal is connected on the upper part to a short fuselage, shaped as the wing and where the connection between the wings takes place, and at the bottom to the cargo bay. In the middle of the pedestal, a cylindrical pocket can host both tail boom and the connecting tube to engine pod (this latter can be disassembled to fit in the transportation box). The intention behind this configuration was to keep the air flow to the wing as clean as possible. Inside the upper

part of the fuselage there is enough space to install the receiver, its battery and the GPS unit. As already mentioned in Section 3.4, the cargo bay centre is coincident with the airplane CG in order to avoid any CG displacement at variable payload. The blood bags are accommodated inside three compartments that are accessible from the bottom.

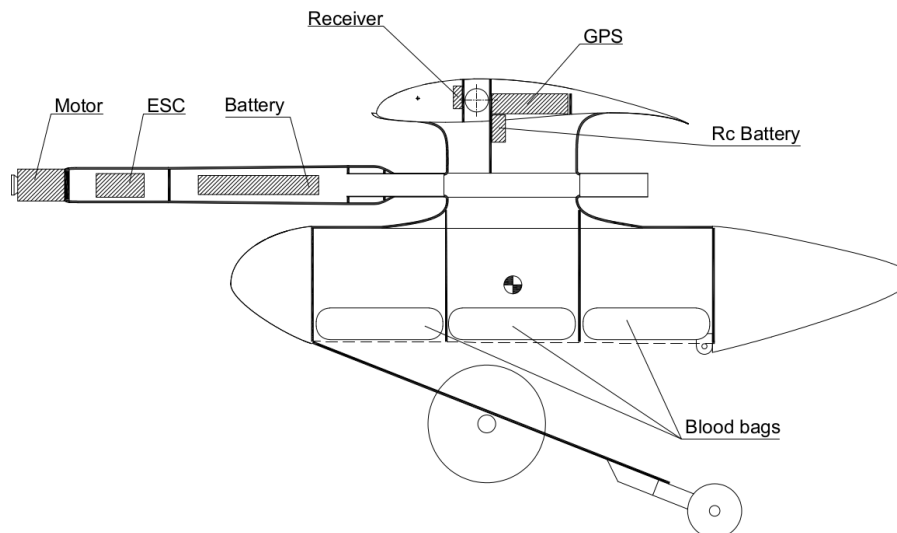


Figure 14: Internal structure of the pedestal

The fuselage bottom plate is indeed hinged at the most forward fuselage bulkhead and secured in locked positions by means of metallic pins. This component holds in place also the main landing gear and tail wheel. The landing gear is made of 10 mm carbon tube that terminates with an aluminium threaded pin where the wheels' bearings can be secured in place by M6 bolts. Two different main landing gear can be installed, they differ by the length of the tube. The shorter one that allows the wheels facing just aside the cargo bay is the best choice to minimize aerodynamic drag. The wider one might be used to ease take off in the event of strong cross wind conditions.



Figure 15: 3D printed main wheel

The wheels are 3D printed in plastic material and their design is the results of many trials at the airfield. A picture of the main wheel final solution is given in Fig. 15. The inner part is made with an honeycomb structure of polyethilen thereftalalte glycol (PETG) and host also the bearing, while the external part is more soft to have more grip and simulate a tyre and is printed out of thermoplastic

polyhuretane (TPU). At the end the total weight of this solution is only 25 g and proved to be sufficiently robust to handle hard landings at MTOW. A similar structure is adopted also for the tail wheel but without the TPU component. However, the team is at work to improve further the wheel design and used materials to gain a better take-off run control.

Fuselage, cargo bay and pedestal, forms a unique structure and cannot be disassembled. The structure is made with a sandwich of carbon fibre of 49 g/m², 3 mm thickness PVC foam, and 25 g/m² glass fibre fabric. Only the cargo bay fairings are made with a single sheet of carbon fibre, since they are used only for a better aerodynamic.

The engine boom is composed by a pod and a carbon fibre tube used for coupling with the pedestal (see Fig. 14). The engine pod must ensure the accessibility to a load bay where engine regulator and batteries have to be located. The only significant load that the engine pod must be able to sustain is substantially the impulsive loads while taxiing or landing to the battery weight (approximately 300 g). The propeller torque and traction are not considered as significant loads. It was therefore decided to manufacture this component again with the vacuum moulding technique applied on a sandwich: 49 g/m² carbon fabric oriented +/- 45 deg, PVC foam of 1.2 mm thickness and again 25 g/m² glass fibre fabric as the internal one. Four bulkheads are installed inside the engine pod to provide additional torsional stiffness and to install the engine.

The choice to connect the engine pod to the fuselage by means of a tube revealed also very useful in the final setting of both prototype and race model. During the design phase it was very difficult to estimate the correct position of the engine pod such to guarantee the desired airplane CG location. For this reason, the connecting tube was left intentionally longer at the beginning to allow moving the engine pod back and forth in search for the right CG configuration.

4.3 Tail boom and empennages

The realization of the V-tail initially started using a classic structure made of balsa ribs, mounted on a 8 mm diameter commercial carbon tube and covered with monokote. This solution has the advantage to be cheap, fast to manufacture and sufficiently light. However, as reported in Section 3.3, their final planform, is almost elliptical and very thin, therefore too complicated to be manufactured with a traditional structure. The final choice was to go for a composite material solution also in this case. The only significant mechanical request to the empennages is to guarantee torsional stiffness, this also in view of the adoption of a full flying configuration. This requirement was achieved by a very light sandwich for the skins made of bidirectional 49 g/m² carbon fabric, PVC foam of 1.2 mm thickness, and 25 g/m² glass fibre fabric as the internal one. Both fabric fibres are oriented +/- 45 deg with respect the span.

The internal structure (see Fig. 16) is made of two composite sandwich ribs to which the pivoting tube (commercial 8 mm diameter carbon fibre tube) and the servomotor can be fixed. A spar runs from the most internal ribs to the tip and it is made of the same sandwich as for the wing. Two additional ribs connect upper and lower skin and contribute to improve torsional stiffness.

The empennages are connected to the fuselage by a tail boom made by a commercial carbon tube with the following fibre orientation for the different layers (as reported by the manufacturer):

- Outer layer: ± 45 deg (3k carbon fibre fabric with plain weave);
- Core layer: 0 deg (uni-directional carbon fibre);
- Inner layer: 30-45 deg (uni-directional carbon fibre);
- Interlayers: very thin glass fabric.

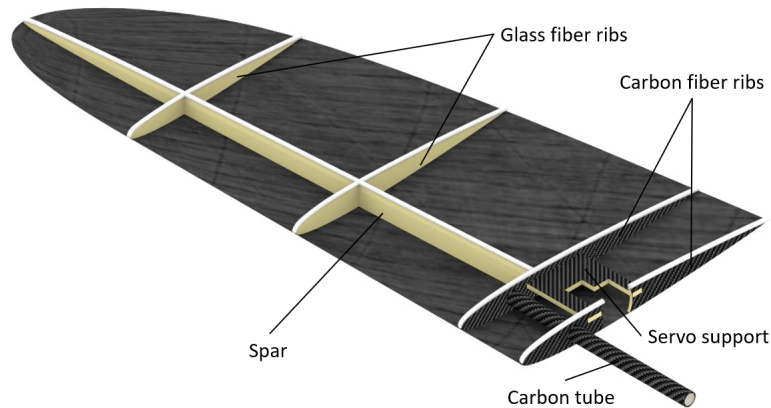


Figure 16: Internal structure of the tail

However, the manufacturer did not specify any mechanical properties. Therefore, the selected tube was subjected to an experimental validation considering the tail boom as a cantilever subject to a vertical force at the free end equal to the maximum lift from the empennage. This latter was taken from the XFLR5 simulations and is about 20 N. The boom was loaded three times this value with no failure and minimum bending. It has however to be mentioned that the main concern about this tail boom and empennage design was the possibility to encounter flutter phenomena. As mentioned, the team had no information available about the tube mechanical properties and, at the same time, flutter instabilities are a rather complicated subject to be treated. To validate the design, the tail boom and empennage were tested in flight on the PH1 prototype model. Flight speeds as high as 35 m/s were reached without any problem. The full reliability of the empennage actuation, which is described in Section 5.2, was also proved.

4.4 Construction process

Vacuum moulding is the technique chosen to realize all the composite components and required some try-outs before reaching the optimal procedure. In particular, the moulds were realized by the team thanks to the availability in the lab of a new CNC 3-axis milling machine (see Fig. 17a).

The team members had to acquire the new skills related to the drawing of complex 3D surfaces and the CAM skills required to generate complex milling paths. This process required several weeks and some trials on the milling machine but at the end allowed the team to spare a significant amount of money (the other option was to give in outsourcing the mould making for an estimated cost of about 1500 euros).

The moulds were machined out from MDF wood and successively were put through a surface treatment, also operated by the team. The treatment consisted of several painting and polishing steps, in order to limit wear from usage and increase surface finishing. The mould's ultimate surface roughness is estimated being around 20 μm , as the final step consisted of P1000-rated sandpaper polishing. As explained in Section 4, three-layer sandwiches are used in the construction. As a core material, PVC foam is used while the external fibre reinforcement can vary depending by the final use. As a matrix, epoxy-F resin of high quality was used. The moulds are left at least 12 h under vacuum and let in a warm room (24 °C or more) for at least 24 h to ensure complete curing of the polymer before any manipulation. The same technique was applied to obtain the laminated panels used to realize the internal structures components.



(a) one of the fuselage moulds at the end of the finishing process



(b) the moulds after the surface treatment

Figure 17: The 3 axis CNC milling machine used for moulds manufacturing

5 Electronics

5.1 Battery sizing

The choice of an appropriate battery was extremely important for the project, it needed to be light to not be a burden to the plane, but it also needed to be electrically adequate to guarantee the expected performance during the flight. Additionally, it had to respect the specifics from the race rules. Those last included having a minimum discharge rate of 30C and a maximum voltage of 12.6 V. The first step for the choice of the battery was to calculate its capacity, to do that an approximated time of flight, and the maximum current absorbed by the motor during that time are required.

The time was calculated as it follows:

- 20 seconds of take-off (i.e. including multiple attempts);
- 60 seconds to reach the maximum altitude;
- 120 seconds to reach the maximum flight travel;
- 60 seconds for landing.

Obtaining a total of 260 seconds. The maximum absorbed current was obtained during the propeller test and resulted in 29.5 A, that was then increased by a factor 1.1 as a security range, so getting a final current of 32.45 A.

With all the required data available, the battery capacity can be computed with the following formula:

$$C = \frac{1000 \cdot I \cdot \Delta t}{3600} \quad (9)$$

where I is the maximum current seen above, Δt is the estimated time of flight in seconds, and the factors 1000 and 3600 are to scale the dimensions in mA and hours. The result was 2343 mAh that was rounded up to 2350 mAh. A large number of 3S-Lipo type batteries were searched on the market and tested in the lab with the engine simulating the flight conditions (260 seconds at full throttle and considering an air speed of about 20 m/s) and monitoring the residual battery voltage during time. An example for three different batteries is provided in Fig. 18.

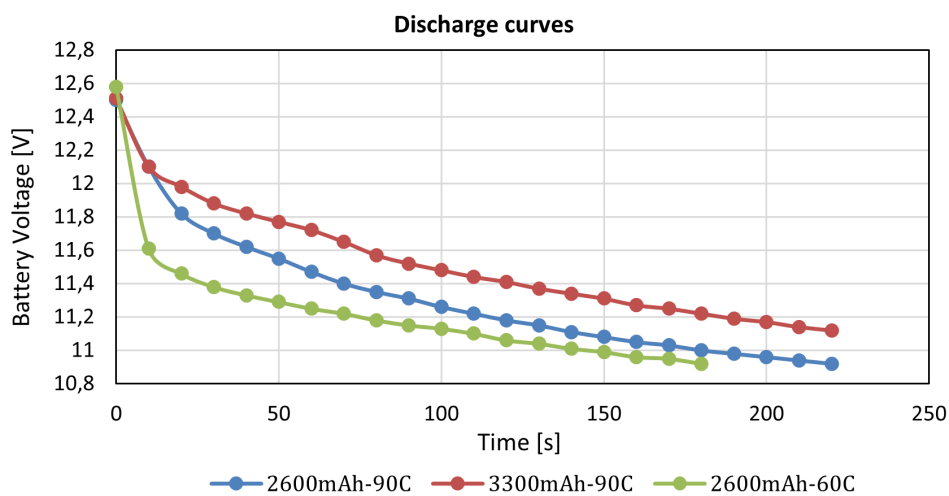


Figure 18: Discharge curves for three different batteries tested

At the end, the choice landed on FullPower Battery Lipo 3S 3300 mAh 90C Platinum, which guarantees all the electric specifications and has an acceptable weight of 302 g. The battery is clearly oversized with respect to both capacity and rated C, but with respect to batteries of lower characteristics, it allows for higher voltage available for a longer time with a moderate increase of weight. Higher voltage means higher rpm and therefore more traction, which is extremely important especially during takeoff and climbing.

5.2 Servomotor sizing

Particular care has been put in the installation of the servomotors and linkages to the control surfaces with the aim to minimize as much as possible the aerodynamic drag. For the ailerons in the wing, a solution was found in the system depicted in Fig. 19. It is a commercial support for servomotor that allows the installation of all the mechanism inside the aerodynamic body. From a kinematic point of view, the system can be modelled as a four-linkage mechanism, as represented again in Fig. 19.

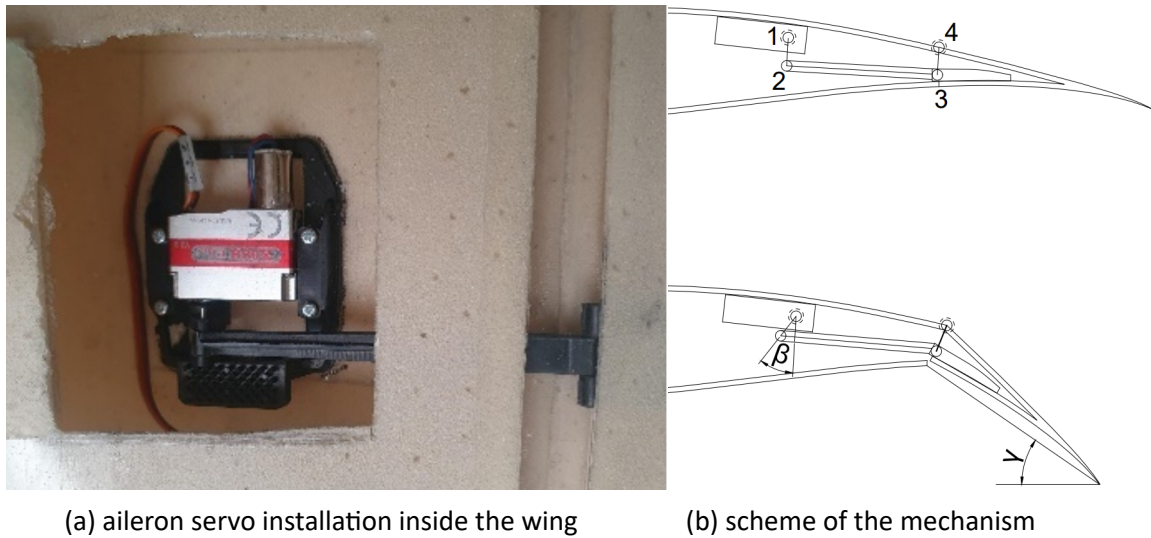


Figure 19

Joint 1 is the servo motor, joint 4 is on the hinge (pressure side) and joint 3 is on the opposite side, so in other words the length of the bar 4-3 is fixed by the wing dimension. In order to compute the required servomotor torque, the following assumptions are made:

- the angle of incidence of the wing is zero and the airflow is considered as non-compressible flow;
- in the neutral position, links 1-2 and 3-4 are parallel;
- friction is negligible.

Starting from the dynamic pressure that act on the air foil, the servomotor torque can be calculated as:

$$T = \frac{1}{4} \rho v^2 c_c^2 L_c \sin \gamma \frac{\tan \gamma}{\tan \beta} \quad (10)$$

where $\beta = 60$ deg in the worst case, and γ depends by link lengths, anyway it always between 30 deg and 40 deg, C_c is the mean chord of the aileron, L_c is its span, ρ is the air density (assumed 1.2 kg/m^3) and v is the flight speed assumed for safety equal to 30 m/s.

The geometrical parameters and the estimated torque are specified in Tab. 3:

Table 3: Geometrical parameters and estimated torque

Control Surface	Average chord (c_c) [m]	Length (L_c) [m]	Torque [kg·cm]
Aileron	0.071	0.300	1.3

A similar approach could be used to size the servomotors in the full-flying V-tail. The schematics of the mechanism is the depicted in Fig. 20. Joint 1 is the hinge, joint 2 is the servo motor that is installed fixed inside the aerodynamic surface, joint 3 is a sliding joint realized on the tail boom.

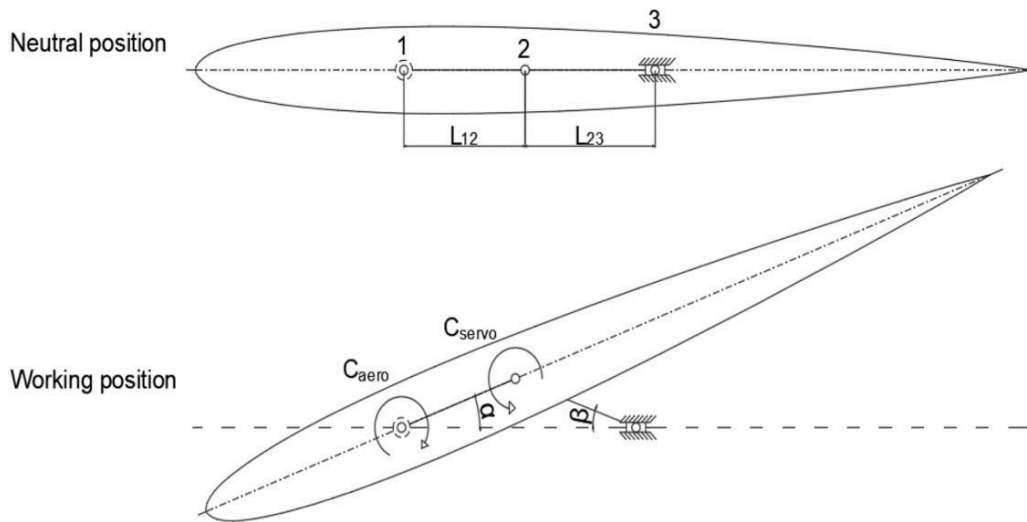


Figure 20: Schematic of the servomotor mechanism for the full flying V-tail

The aerodynamic forces that act on the tail can be calculated assuming that:

- air flow is incompressible;
- the angle of incidence is zero at the neutral position;
- the maximum torque is at α max (10 deg).

Assuming that the aerodynamic forces act at $1/4$ of the mean chord of the tail, by the drawings it is possible to deduce the distance between the first joint and the force application point. The aerodynamic forces (C_{aero}) have been evaluated by the profile polar curves for an incidence angle of 10 deg and at Reynolds number of 250'000.

The servomotor torque can be computed as:

$$Torque = C_{servo} = C_{aero} \left(1 - \frac{l_{12} \cos \alpha}{l_{23} \cos \beta} \right)^{-1} \quad (11)$$

Table 4: Parameters of the tail servos

Tail	l_{12} [mm]	l_{23} [mm]	C_{aero} [Nm]	α [deg]	β [deg]	Torque [kg·cm]
	28.6	14	0.44	10	36	0.31

The chosen servomotors for both ailerons and empennages are 'KST X08H Plus' which guarantee a 3.9 Kg·cm torque at 6 V. The available torque is much higher than the required, but the selected servos are characterized by high precision and stable positioning, quality that are essential for a smooth flight path and to keep the surfaces in the neutral position when not activated.

5.3 Flight Telemetry

The addition of automatic measurements of altitude and position to determine the flight score is one of new features implemented by this year ACC rules. The team took immediately the decision to develop the necessary tool to be able to evaluate their models' performance and identify a possible

race strategy. The same GPS hardware that will be used in competition has been bought (SM Modellbau Gps Logger 3) and a MATLAB tool was developed to extract the information that are requested to compute the score accordingly to race rules. A screen shot of the software with the logged data from a test flight is shown in Fig. 21.

The software displays the altitude profile during flight, the vario data (computed as temporal derivative of the altitude) and the aircraft's speed. Actual computation of the score is given in output by providing payload value and take-off distance (bonus points if less than 40 m).

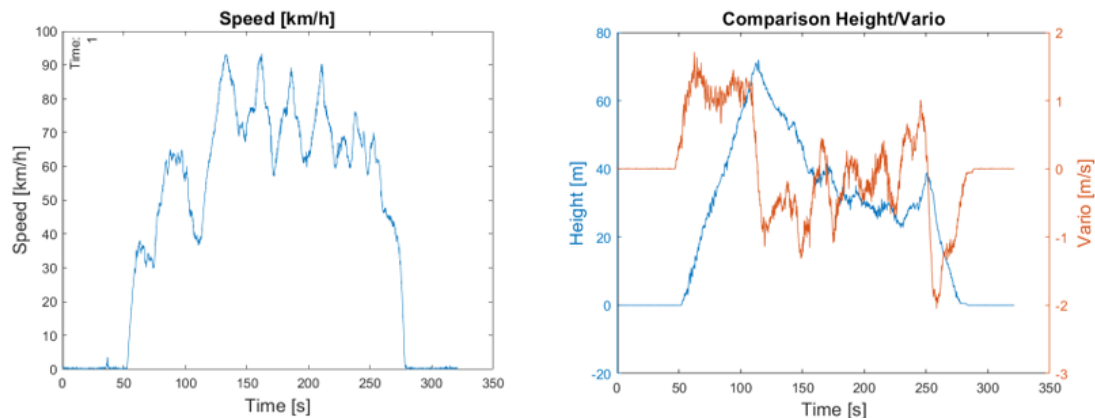


Figure 21: Example of MATLAB telemetry plots

The GPS data are delivered to the telemetry system of the remote controller and displayed live on the TX screen. These information (in particular the actual altitude) are read by the pilot helper and proved to be extremely useful for a successful flight attempt.

In addition to the GPS and with the aim to improve the flight path from a race point of view, the air speed velocity was also added to the set of measurements. A Pitot tube was installed at the wing tip of the BcdM1 prototype and connected to a Futaba Telemetry Air Speed Sensor SBS-01TAS. Having a rough indication of the true air speed combined with the value of the ground air speed (by the GPS) it was judged to be useful in determining the effect of wind on the flight path, especially if the climbing phase is concerned.

The air speed sensor has no data storage capability, so to log all the data the Futaba Transmitter was used. The Futaba Transmitter has the possibility to store the telemetry data it receives from any sensor connected to the receiver, by saving them on a SD card. The logs are saved in a .FDI format that need to be converted in a .csv using the proprietary software Futaba Telemetry Log Converter. After data format conversion, it's possible to elaborate all the data using the MATLAB routine. However, some additional pre-processing on air speed data is necessary because:

- the sampling rate of the air speed sensor is lower (1 Hz) with respect to that of the GPS (set at 10 Hz);
- air sensor sampling is affected by an important jitter causing the sampling period to have variations up to 50% the nominal sampling time;
- data storage starting time is different between air speed sensor and GPS.

These problems were easily solved by a re-sampling of the airspeed data and a cross comparison of the GPS log time on the TX and GPS itself.

6 Optimization process

The aerodynamic design methodology described in Section 3 is obviously quite simplified and does not take into account a number of variables and their interaction and effects on the final performances. Similar arguments can be made about the structural design approach. The team was therefore conscious that the developed design could not be the best possible but however it was difficult to dedicate more time and resources to a more accurate approach (again because of the situation imposed by the pandemic and the small number of teammates). This are the reason behind the decision to proceed with an “experimental approach”: build a first prototype to proof the most important aspects of the design (e.g. wing and tail aerodynamics) and then concentrate on structure and flight performance optimization, eventually by building a second prototype before the race model was completely define. This section aims at exposing briefly the mail stone of this process.

6.1 The first prototype BcdM1

Fig. 22 shows images of the first prototype BcdM1. Wings were manufactured in composites out of the moulds that are currently used to manufacture the final version. Mechanical resistance of the wing had to be of no concern for this prototype, as for the total empty weight. Therefore, the composite sandwich was realized with glass fabric of 80 g/m^2 (available as spare in the lab from another project) and also reinforced under the spar with unidirectional carbon tape. Tail surfaces were realized with a classical structure with ribs and covered with monokote, sufficient to reach the target that was to verify the correct design in terms of memorability, static stability and reliability of the full flying V-tail configuration. The fuselage was built out of plywood, the cheapest and fastest possible solution. The airplane empty weight was at end equal to 4530 g.

The prototype was successfully maiden at the end of September 2020 and after numerous test flights, it was clear that the target performance could be reached as soon as fuselage aerodynamic and empty weight would have been improved.

6.2 The second prototype PH1

After the flight tests of BcdM1, the design of the new airplane began, facing problems such as the location of the cargo bay, the way the payload can be rapidly loaded or unloaded, improve the overall aerodynamic, reduce the empty weight, etc.

After few months of design and construction, the PH1 model was ready for its first flight at the end of 2021, see Fig. 23. The team was very satisfied of the work carried out up to that point and started thinking that the PH1 model could have been the race one, ready in large anticipation with respect the schedule and without the need of further substantial modifications that would have required a new airplane. This, as it will be clarified later on, was not the case.

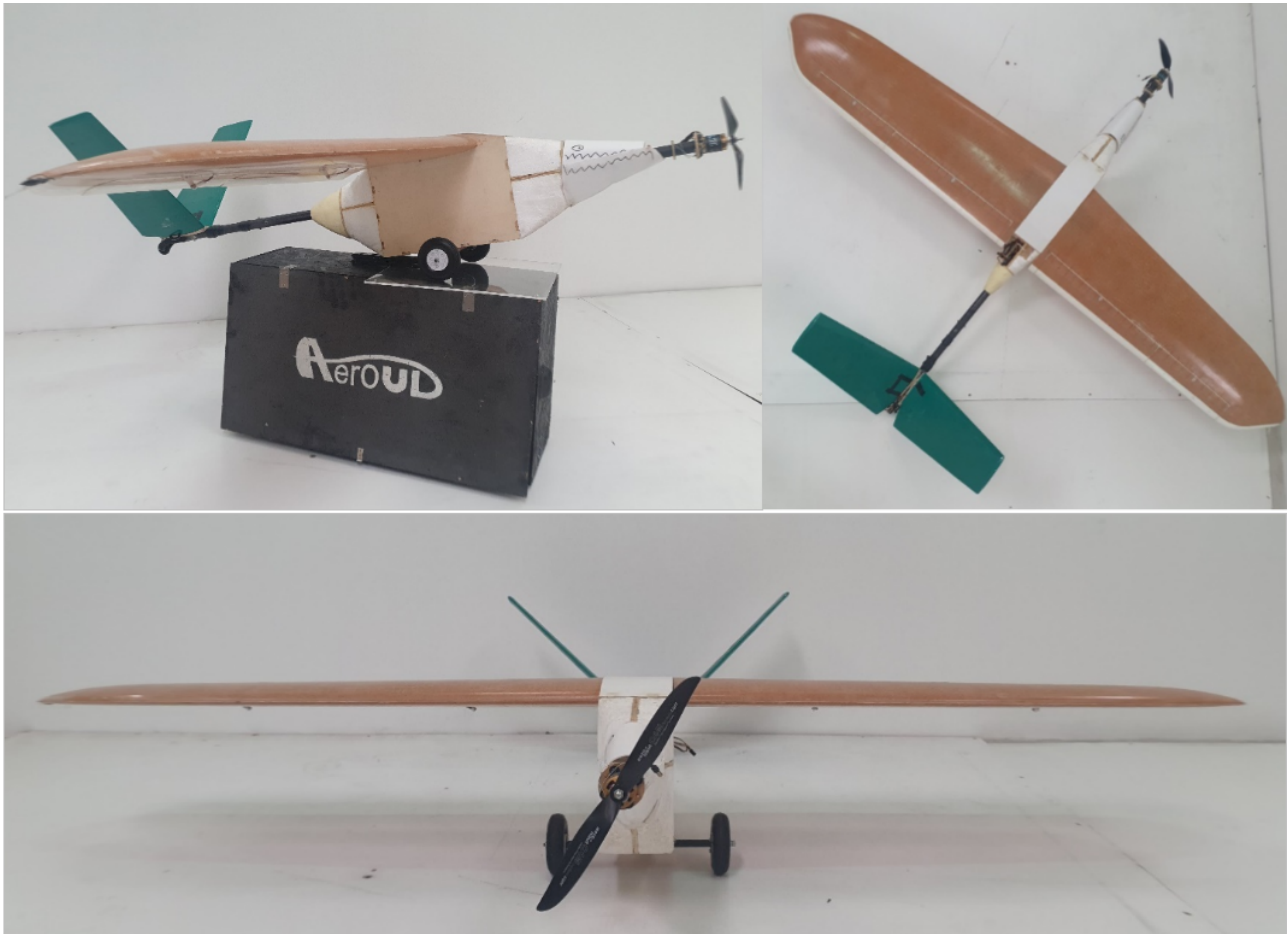


Figure 22: The BCdM1 prototype



Figure 23: The PH1 prototype

The first goal was successfully reached: the empty weight of the airplane was reduced to 2350 g, way lower than the team expectations. The flights carried out at the maximum of the payload the airplane was able to carry (11 bags of 300 g) proved the mechanical resistance of the structure, as well as any doubts about possible flutter problems of the tail were also cancelled.

The most important result of the flight test campaign was that the airplane was actually able to carry more payload than the 3300 g it was design for. In addition, the original project considered the adoption of wing flaps to improve short takeoff capabilities. Flight tests demonstrated that the flaps bring a modest advantage in terms of takeoff distance (few meters) and conversely penalizes the climbing phase. Indeed, the model needs some time to accelerate to optimal climbing speed as soon as flaps retraction has been operated, which in turns penalizes the reached altitude in 60 seconds.

It was therefore decided to redesign the cargo bay to accommodate one more 300 g bag (from 11 to 12 total bags), consider lighter but still performant servomotor for both ailerons and empennages (see Section 5.2) and not to install flaps. In this way a saving of about 120 g from the empty weight will be realized, saving that should cover the increase associated to a larger cargo bay. These are the main differences between the PH1 and the race model PH2 currently under construction.

PH1 several flights were also useful to figure out the best solution for the wheels and constructions of the main landing gear. Position of the main carriage was carefully chosen as compromise to ease the tail lift at MTOW and to avoid pitching nose down (because of the irregularity of grass runway) at lower weights. Also, the airplane suffers significantly cross wind conditions during take-off in view of the large side area of the cargo bay. This problem was partially solved by adopting a wider main landing gear (larger distance between the wheels) that helps to prevent from rolling downwind.

The data logged at MTOW and in different days (from October 2021 to March 2022) helped in the definition of the payload prediction chart.

7 Payload prediction

Payload prediction chart is based on data from test flights and propeller traction data. During the flight tests, the average aircraft speed was measured by means of a GPS telemetry module, by taking also into account possible effects of wind. This data, together with the knowledge about air density value at those days and airplane take-off weight, allow us to determine experimentally the actual lift coefficient, that is kept constant for the estimation of the payload. Propeller performance data is scaled based on the actual air density value and so, from dynamic equilibrium (traction propeller = drag), it is possible to determine a new flight speed for every air density condition. The regulation requires that payload prediction have to be calculated as a function of the air density, with the following linear approximation:

$$P = 1.515 \cdot \rho + 1.414 \quad (12)$$

where ρ is the density altitude and is expressed in $[\text{kg}/\text{m}^3]$, and P is the predicted payload in $[\text{kg}]$. The function is also plotted in Fig. 24.

The prediction was also verified in occurrence of flight tests with different density altitude.

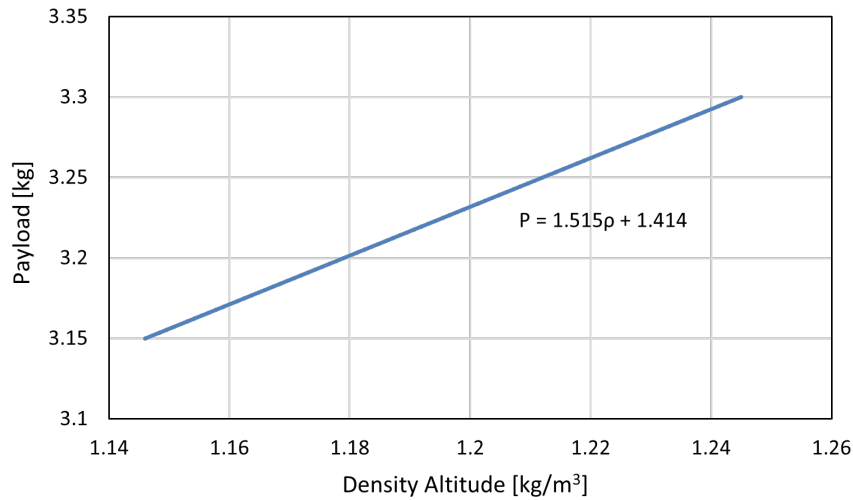


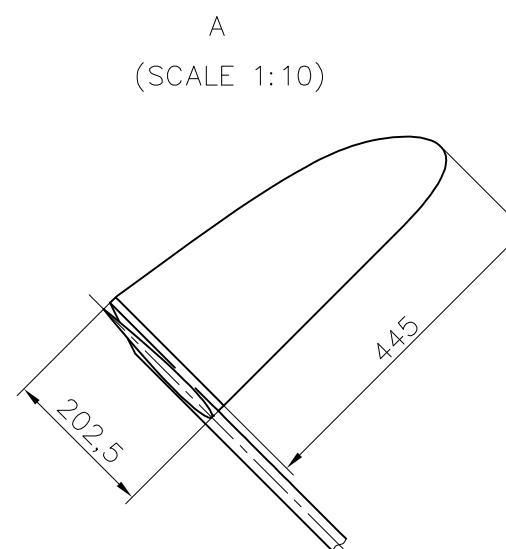
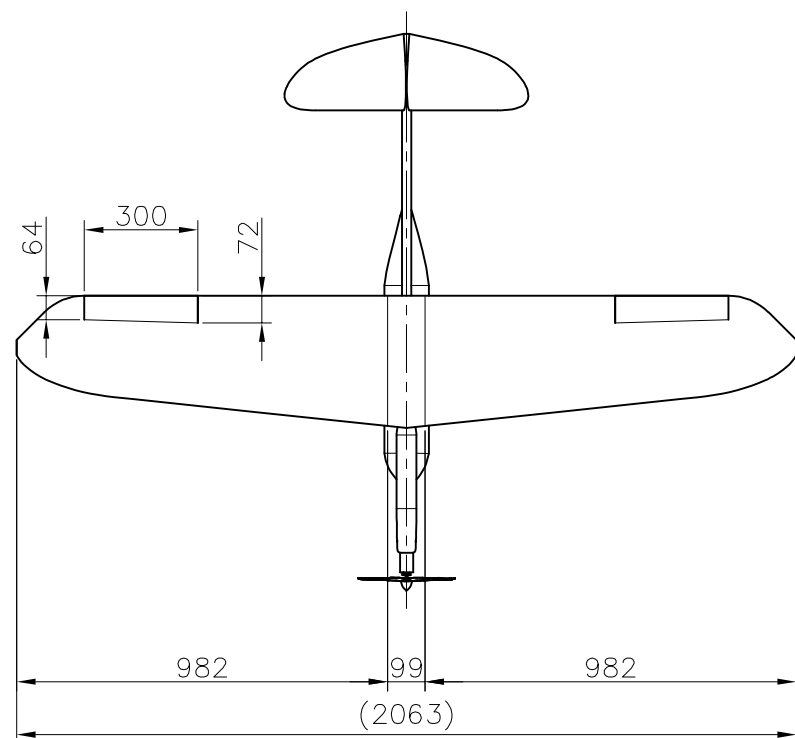
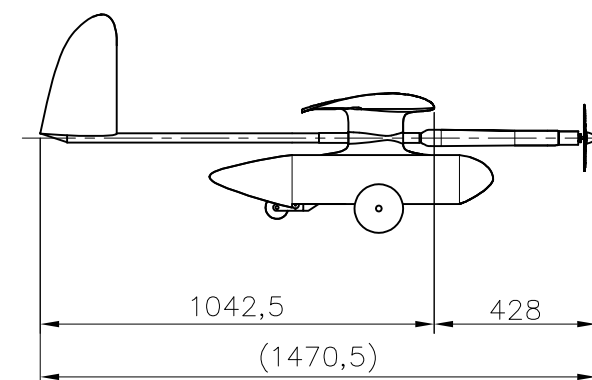
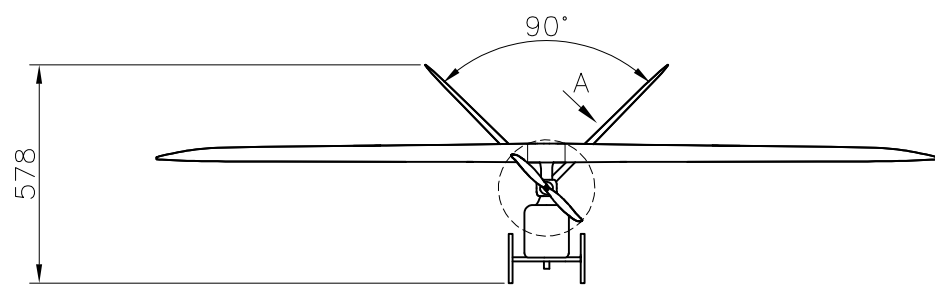
Figure 24: Payload prediction chart

8 Outlook

With the present report, the team aims providing to the jury a thorough overview of the challenging path that was undertaken to get ready for the race. For this reason and within the limits of the available pages, only the major and qualifying aspects were reported. During the design and construction period the team had to deal with many difficulties, mostly related to the organization of the activities in lab. This was due to the limitations imposed by the pandemic outburst of COVID, which prevented a regular in-presence activity. Taking into account the above considerations, it became clear the need to simplify as much as possible the design approach in order to make the project feasible on time and with the available resources.

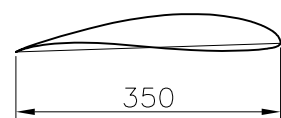
Despite these difficulties, the team believes that the competition aircraft is going to reach good performances, thanks to the intense optimization process mostly based on the analysis of data collected during the flight test campaigns.

At the present time, the competition aircraft is undergoing the completion phase. In the remaining months before ACC2022, the team will define and optimize a race strategy by doing multiple flight tests. These months will also be used to complete the video report.



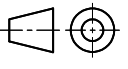
Airfoil – SCALE 1:10

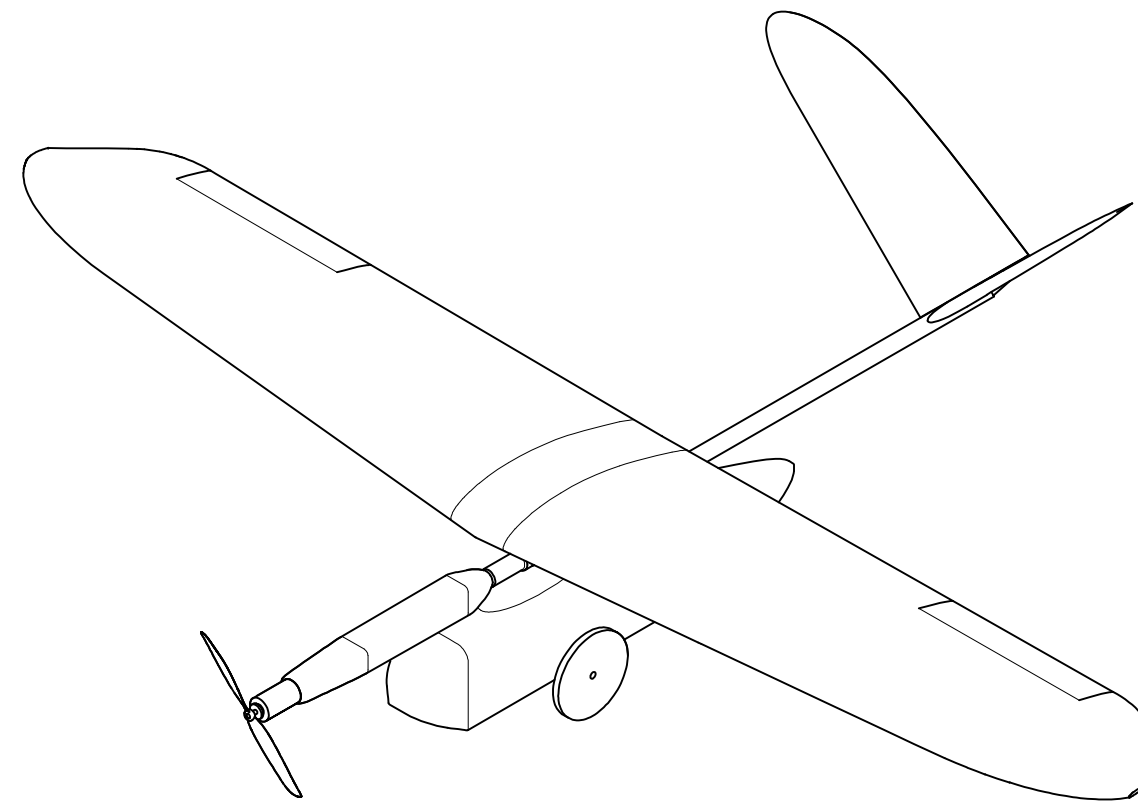
Wing airfoil at the root
(Wortmann FX 63-137)



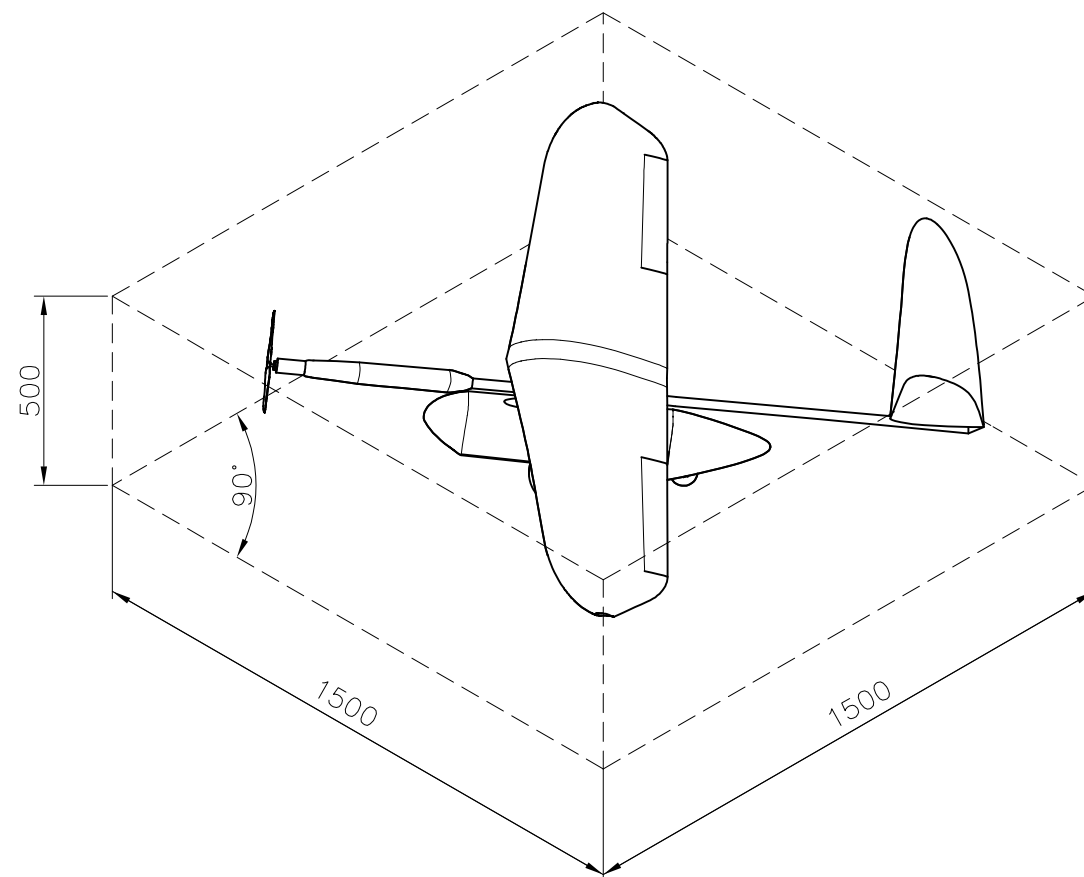
Tail airfoil at the root
(NACA0009)

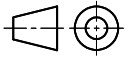


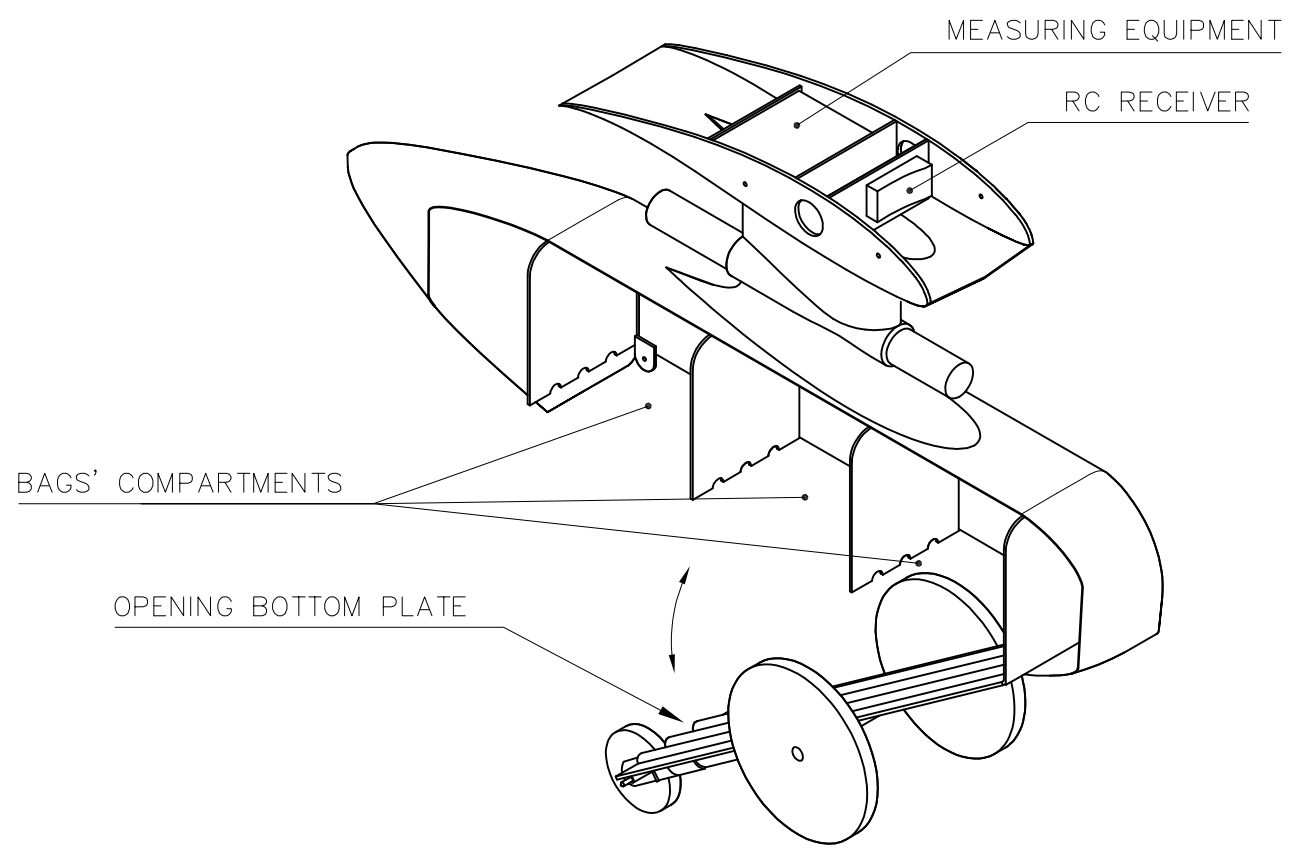
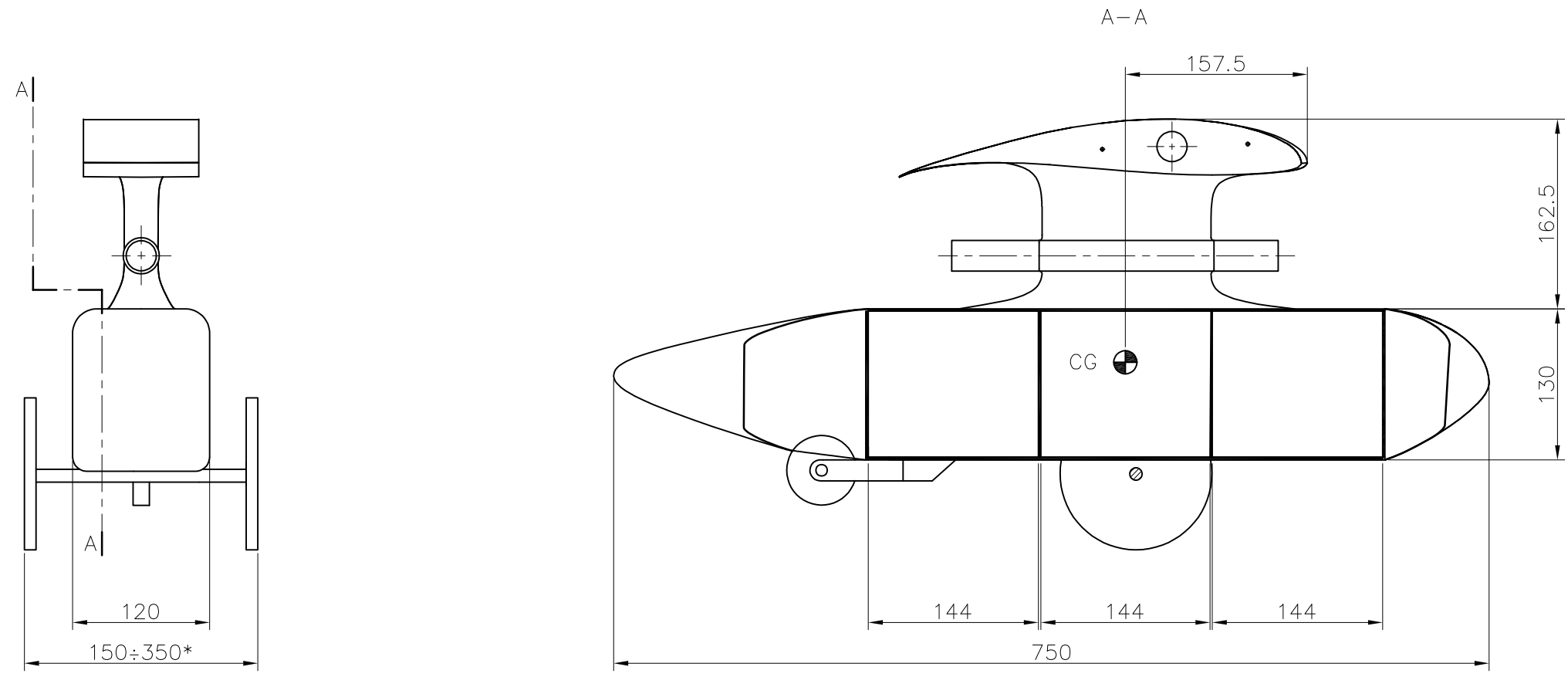
Surface		Area
Wing		0.584 m ²
Aileron		0.020 m ²
Full-flying Tail		0.136 m ²
 UNIVERSITÀ DEGLI STUDI DI UDINE		TITLE 3-VIEW DRAWING
FORMAT A3		TEAM'S NAME - NUMBER AEROUD - 12
SCALE 1:20	DATE 06/04/2022	GENERAL TOLLERANCES UNI EN-ISO 22768-1-v
DESCRIPTION - front view at the top left corner - top view below - starboard view at the top right		



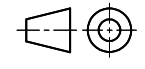
(SCALE 1:20)

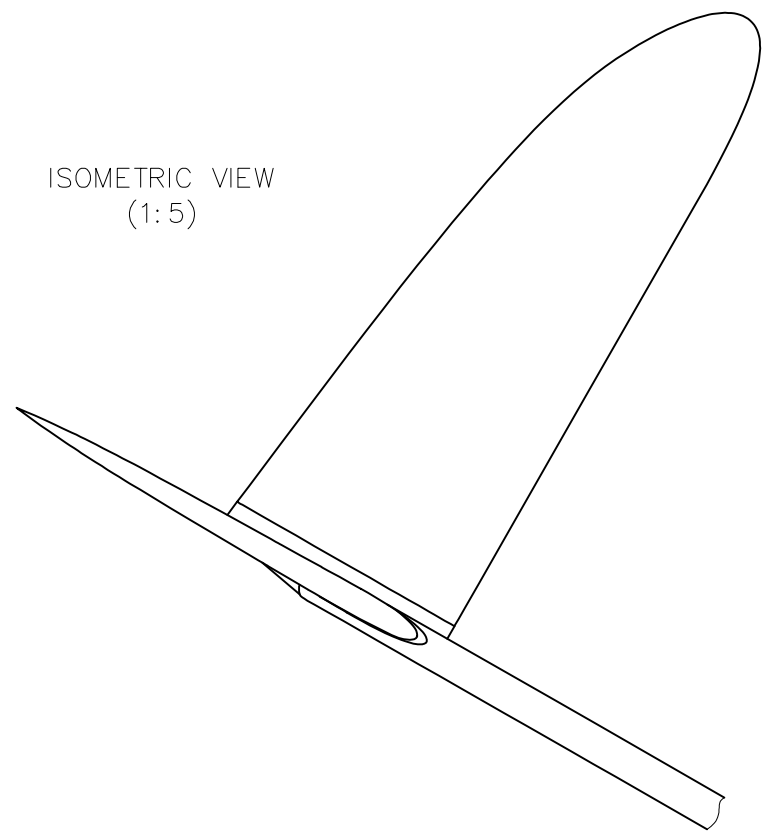
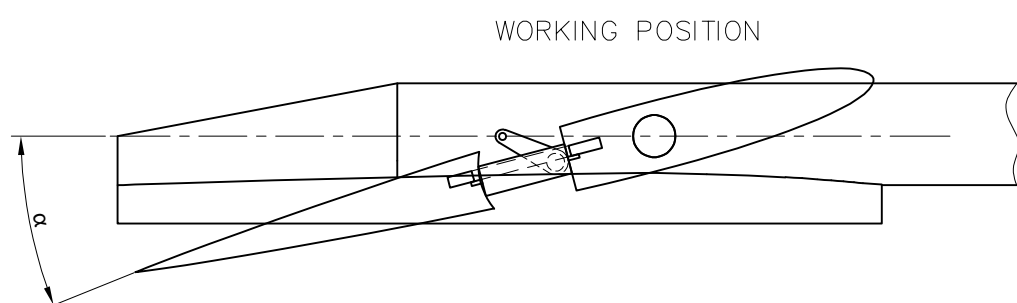
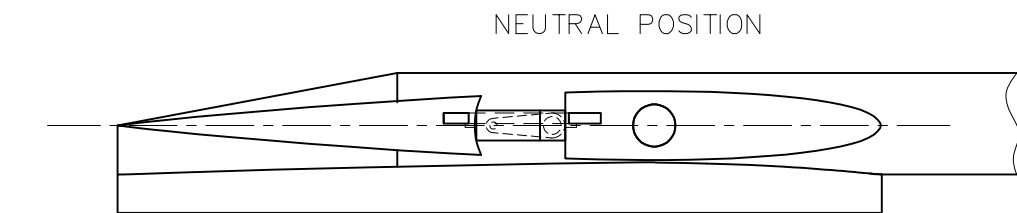
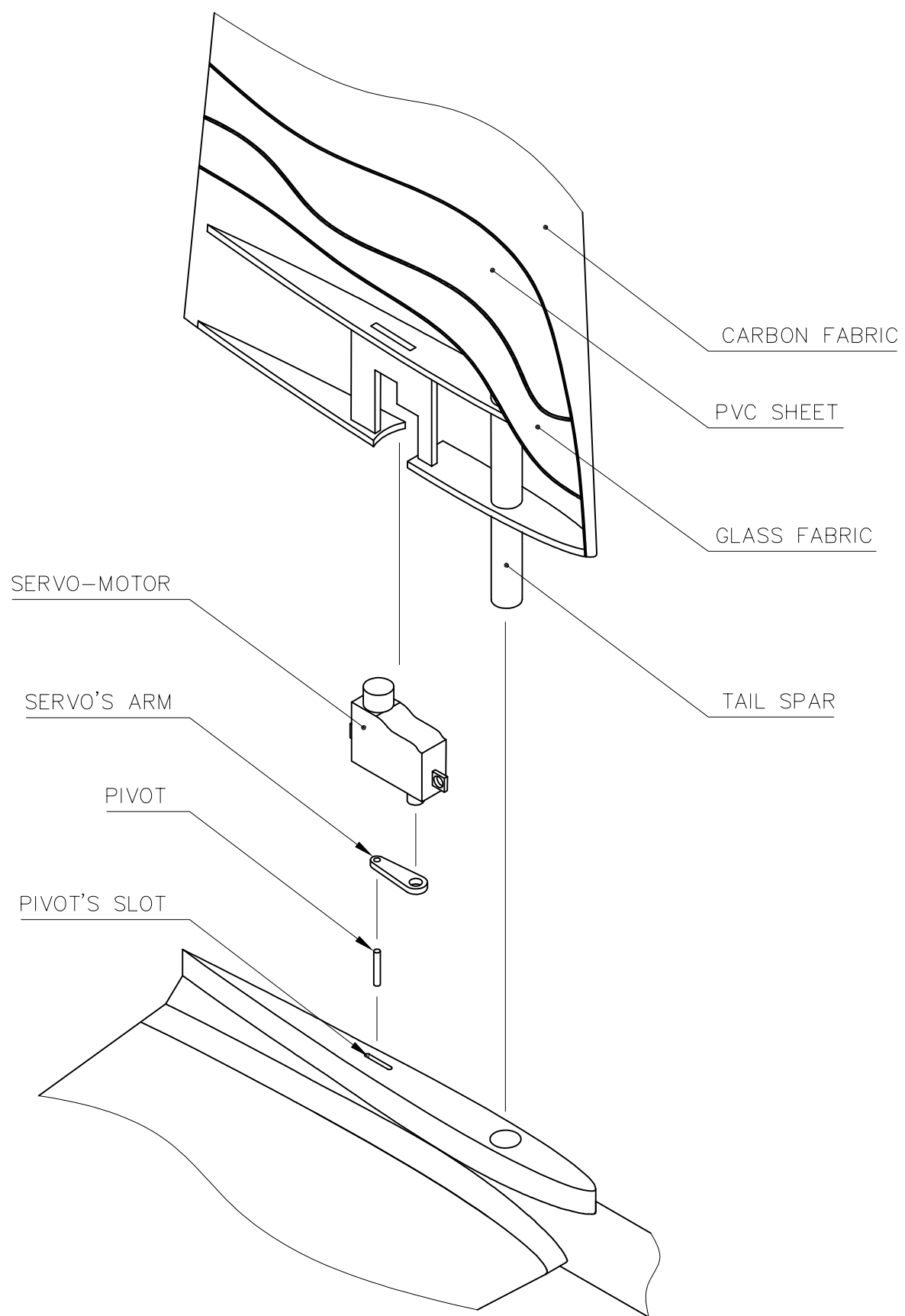


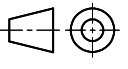
 UNIVERSITÀ DEGLI STUDI DI UDINE		TITLE ISOMETRIC PERSPECTIVE VIEW	
FORMAT A3		TEAM'S NAME - NUMBER AEROUD - 12	GENERAL TOLLERANCES UNI EN-ISO 22768-1-v
SCALE 1:10	DATE 06/04/2022	DESCRIPTION Isometric perspective view	



(*) Landing gear's length range depending on take-off condition

 UNIVERSITÀ DEGLI STUDI DI UDINE		TITLE CARGO BAY	
FORMAT A3		TEAM'S NAME - NUMBER AEROUD - 12	GENERAL TOLLERANCES UNI EN-ISO 22768-1-v
SCALE 1:5	DATE 06/04/2022	DESCRIPTION - Cargo bay location and principal dimensions - Location of the RC reciver and the measuring equipment	



 UNIVERSITÀ DEGLI STUDI DI UDINE		TITLE FULL-FLY TAIL	
FORMAT A3		TEAM'S NAME - NUMBER AEROUD - 12	GENERAL TOLLERANCES UNI EN-ISO 22768-1-v
SCALE 1:2	DATE 06/04/2022	DESCRIPTION Full-flying tail and explanation of how it works	